# DIA-MS proteome analysis of formalin-fixed paraffin-embedded glioblastoma tissues

Analytica Chimica Acta 1204 (2022) 339695

Contents lists available at ScienceDirect

Analytica Chimica Acta

journal homepage: www.elsevier.com/locate/aca

# DIA-MS proteome analysis of formalin-fixed paraffin-embedded glioblastoma tissues

Kenneth Weke [a, 1], Sachin Kote [a, **, 1], Jakub Faktor [a], Sofian Al Shboul [e], Naomi Uwugiaren [a], Paul M. Brennan [d], David R. Goodlett [a, c], Ted R. Hupp [a, b], Irena Dapic [a, *]

[a] International Centre for Cancer Vaccine Science, University of Gdańsk, Gdańsk, Poland
[b] Institute of Genetics and Cancer, University of Edinburgh, Edinburgh, Scotland, UK
[c] Genome BC Proteomics Centre, University of Victoria, Victoria, British Columbia, Canada
[d] Translational Neurosurgery, Centre for Clinical Brain Sciences, Bioquarter, University of Edinburgh, Edinburgh, UK
[e] Department of Basic Medical Sciences, Faculty of Medicine, The Hashemite University, Zarqa, Jordan

## HIGHLIGHTS

- DIA-MS workflow for the analysis of glioblastoma FFPE stissue samples.
- Detection and quantification of glioblastoma-relevant proteins in FFPE tissues.
- Quantification of immune-related proteins in glioblastoma tissue samples.
- The workflow revealed glioblastoma patient-specific proteome and can be globally applied to other FFPE tissues.

## GRAPHICAL ABSTRACT

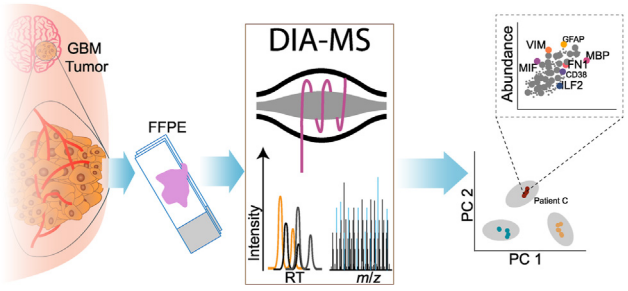


## ARTICLE INFO

*Article history:*
Received 5 November 2021
Received in revised form
4 March 2022
Accepted 5 March 2022
Available online 12 March 2022

*Keywords:*
Data-independent acquisition
Quantitative proteomics
Formalin-fixed paraffin-embedded
Glioblastoma
Mass spectrometry

## ABSTRACT

Developments in quantitative proteomics and data-independent acquisition (DIA) methodology is enabling quantification of proteins in biological samples. Currently, there are a few reports on DIA mass spectrometry (MS) approaches for proteome analysis of formalin-fixed paraffin-embedded (FFPE) tissues. Therefore, to facilitate detection and quantification of immune- and glioblastoma (GBM)-relevant proteins from FFPE patient materials, we established a simple and precise DIA-MS workflow. We first evaluated different lysis buffers for their efficiency in protein extractions from FFPE GBM tissues. Our results showed that more than 1700 proteins were detected and over 1400 proteins were quantified from GBM FFPE tissue microdissections. GBM-relevant proteins (e.g., GFAP, FN1, VIM, and MBP) were quantified with high precision (median coefficient of variation <12%). In addition, immune-related proteins (e.g., ILF2, MIF, and CD38) were consistently detected and quantified. The strategy holds great potential for routinizing protein quantification in FFPE tissue samples.



* Corresponding author. International Centre for Cancer Vaccine Science, University of Gdańsk, Kładki 24, 80-822, Gdańsk, Poland.
** Corresponding author. International Centre for Cancer Vaccine Science, University of Gdańsk, Kładki 24, 80-822, Gdańsk, Poland.
*E-mail addresses:* sachin.kote@ug.edu.pl (S. Kote), irena.dapic@ug.edu.pl (I. Dapic).
[1] These authors contributed equally.

https://doi.org/10.1016/j.aca.2022.339695

## 1. Introduction

Mass spectrometry (MS)-based proteomics is currently the last frontier for comprehensive characterization of proteins and their functional changes. The data-dependent acquisition (DDA) strategy has been primarily used to detect and quantify proteins for a long time. However, due to insufficient proteome coverage and reproducibility occasioned by the stochastic sampling of the most intense peptide ions, the quantitative proteomics field is now shifting to data-independent acquisition (DIA) methodology [1–4]. DIA-MS is based on a full scan of all precursors that are subsequently isolated and fragmented within a defined mass to charge ($m/z$) window until the scanning covers the entire $m/z$ range of the initial full scan [5–7]. DIA-MS has demonstrated high reproducibility and precision in protein quantification [8]. It has been successfully applied so far on freshly frozen (FF) and formalin-fixed paraffin-embedded (FFPE) tissue samples (Table 1). Thus, DIA-MS is increasingly becoming popular in quantifying proteins in clinical samples [9–13].

However, the application of DIA-MS on FFPE is still limited compared to DDA-MS. FFPE samples from diagnostic laboratories are of particular interest for retrospective studies since they have considerable follow-up data useful for correlating observed clinical outcomes with patient-specific proteome. In addition, formalin fixation and paraffin embedding is a routine method for tissue preservation, and their regular collection, long-term stability make them easily accessible for large cohort studies [14]. Therefore, effective proteomics analysis of FFPE is critical to the study of clinically-relevant proteins and the discovery of novel protein biomarkers for early disease detection and prediction of clinical outcomes. Recently, the use of DIA-MS on clinical FFPE samples facilitated tumor stratification and enabled the discovery of potential biomarkers for prostate cancer [15]. While FFPE specimens remain more appealing for retrospective investigations than FF tissues, they present a challenge for proteomics analysis due to introduced protein crosslinks during the fixation process. Thus, effective protein extraction from the FFPE tissues is crucial for successful analysis.

Effective extraction of proteins from FFPE samples requires reversing the formaldehyde-induced crosslinks. Some of the methods described used heat-induced antigen retrieval (HAIR) [16,17] to achieve this. Numerous protocols have been published for protein extraction from human tissues for subsequent LC-MS analysis. Extraction buffers are used with the main goal to successfully solubilize and denature proteins. Some of the buffers as primary amine-containing buffer such as ammonium bicarbonate (ABC) are often supplemented with chaotropes (e.g., urea or guanidine hydrochloride), organic solvents (e.g., acetonitrile (ACN) or trifluoroethanol), and/or detergents (e.g., RapiGest, sodium dodecyl sulfate or sodium deoxycholate) all to achieve good protein extraction [18–23]. In Table 1, we have briefly highlighted several protein extractions and digestion protocols, including in-solution digestion (ISD) [24,25], direct trypsinization (DT) [19,20,26], filter-aided sample preparation (FASP) [22,27], and single-pot, solid phase-enhanced sample preparation (SP3) [28] for FFPE tissue proteomics. To date, protein retrieval with ISD protocols and optimized chemical buffers is a typical workflow in tissue proteomics. Therefore, a critical assessment of chemical buffers is crucial prior to establishing the most effective workflow for MS-based proteome analysis of FFPE tissue samples.

Herein we present a study focused on establishing a simple DIA-MS workflow for detecting and quantifying immune- and GBM-relevant proteins in patient-derived FFPE microdissected tissue samples. GBM is a cancer of unmet clinical needs with a median survival rate of less than two years [29]. In addition, it exhibits high molecular heterogeneity [30,31], which complicates its biology. Therefore, to ramp up studies on complex tumors such as GBM, simple, highly precise, and easily implementable proteomics methods are necessary. Here, we compared the efficiency in protein extraction of three different buffers to find the best conditions for protein isolation and digestion. Consequently, we determined if single-shot DIA-MS using ~10 $mm^2$ (15 μm thick) GBM FFPE tissue sections would precisely quantify the expression levels of relevant proteins. As a result, we detected and quantified GBM-relevant proteins such as fibronectin 1 (FN1), vimentin (VIM), and myelin basic protein (MBP) from the DIA-MS data. Additionally, immune-relevant proteins such as C3, CD47, CD38, interleukin enhancer-binding factor 2 (ILF2), macrophage migration inhibitory factor (MIF) were also quantified. Thus, this approach offers novel opportunities for accelerating biomarker discovery using patient-derived FFPE samples.

## 2. Materials and methods

### 2.1. FFPE tissue samples

Tissue samples used in this study were acquired from human GBM patients (n = 5) according to local ethical approvals (University of Edinburgh, Edinburgh Cancer Research Centre, reference number 06/S1101/16). All ethical requirements regarding using

**Table 1**
A brief highlight of tissue proteomics studies using DIA-MS or DDA-MS.

| References | Tissue origin and amount | Buffer components | Column type | Mass spectrometer | # of identified proteins |
|---|---|---|---|---|---|
| Marchione et al. [13] | human FFPE liver, 1 mm thick | 5% SDS 100 mM Tris pH 8.5 | 20 cm x 75 μm i.d | Q Exactive HF-X, (DIA-MS) | 3,297 |
| Hou et al. [4] | human FF esophageal squamous cell carcinoma | 2% SDS, 7 M urea, 10 mM EDTA, 0.1 M Tris-HCl, pH 7.6 | 50 cm x 75 μm i.d | TripleTOF 5600+, (SWATH-MS) | 1,758 |
| Kim et al. [10] | human FF colorectal cancer tissue, 1 μg | Liquid Tissue buffer | 10 cm x 100 μm i.d | TSQ Quantiva, (DIA-MS) | 3,713 |
| Gao et al. [12] | human hepatocellular carcinoma tissue, 0.2 g | 50 mM Hepes, 6 M urea, 2 M thiourea, 1 x protease inhibitor | 15 cm x 75 μm i.d | TripleTOF 5600+, (SWATH-MS) | 4,216 |
| Pirog et al. [21] | human GBM, 15 μm thick | 100 mM ABC, 30% ACN (PCT) | 21 cm x 75 μm i.d | TripleTOF 5600+, (DDA-MS) | 998 |
| | | 1% SDS, 0.1 M Tris pH 7.6 (FASP) | | | 700 |
| | | 8 M urea, 30% ACN, 100 mM ABC (ISD) | | | 1,233 |
| Föll et al. [20] | mouse kidney, 10 μm thick | 0.1% RapiGest, 0.1 M HEPES pH 8, 1 mM DTT (DT) | 15 cm x 50 μm i.d | Orbitrap Q-Exactive plus, (DDA-MS) | 1,841 |
| | | 4% SDS, 0.1 M HEPES pH 7.5, 0.05 M DTT (FASP) | | | 1,857 |

HEPES - 4-(2-Hydroxyethyl)piperazine-1-ethanesulfonic acid.
Tris - Tris(hydroxymethyl)aminomethane.

human specimens for research were taken into account. Informed consent was obtained from patients, and the Royal Edinburgh Hospital Ethics Review Committee approved the study.

### 2.2. Sample collection

GBM FFPE tissue samples were frozen in liquid nitrogen within 60 min of surgical removal and stored at −80 °C. Each FFPE sample was evaluated by a neuropathologist to confirm GBM diagnosis. A set of five GBM tissues were further processed. Three 4 μm, 10 μm, and 15 μm thick FFPE tissue sections were retrieved from each block of GBM tissue.

### 2.3. Sample processing

Glass-mounted FFPE tissue sections were initially deparaffinized and rehydrated prior to applying the various extraction protocols used in the study. FFPE tissue was deparaffinized by using two xylene washes for 2 min each. ACN, ethanol, and water were acquired from VWR-Avantor (PA, USA). Other chemicals, unless otherwise stated, were obtained from Sigma (MO, USA). Tissue rehydration was performed in ethanol series from 100% to 85% and a final 70%, each for 2 min, and followed by placing the glass slide in LC-MS grade water twice for 2 min each. The deparaffinized and rehydrated tissues sections were then scratched off from the glass slide using a clean razor and put into a clean LoBind Eppendorf tube (Merck, Darmstadt, Germany).

Method 1 - (ACN-containing buffer with ISD). Here, the extraction buffer consisting of 50 μL of 30% ACN and 100 mM ABC was added to the samples. The sample-extraction buffer mixture was incubated at 95 °C for 90 min followed by a cooling to 37 °C. Disulfide bonds were reduced by adding 2.8 μL of 700 mM dithiothreitol (DTT) to the sample-buffer mixture and then incubated at 37 °C for 30 min. Alkylation was performed by adding 9.2 μL of 700 mM iodoacetamide (IAA) to the mixture and incubating for a further 30 min at 37 °C in the dark. After incubation, samples were diluted by adding 120 μL of 100 mM ABC and 880 μL of LC-MS grade water. Protein digestion was carried out by adding trypsin (Promega, MA, USA) to each tissue section in a ratio of 5 ng/mm$^2$, and incubated at 37 °C for 17 h. Digestion was quenched by adding 50 μL of 5% trifluoroacetic acid and vortexed for 30 s.

Method 2 - (ACN-urea-containing buffer with ISD). For this protocol, 50 μL of 30% ACN, 100 mM ABC were added to the samples and the mixture was incubated for 90 min at 95 °C. Subsequently, the sample-buffer mixture was cooled down to 37 °C after which, 50 μL of 8 M urea was added. Next, 5.6 μL of 700 mM DTT was added to the mixture, followed by a 30-min incubation at 37 °C. For alkylation, 18.4 μL of 700 mM IAA was added and the sample was incubated for 30 min at 37 °C in the dark. Samples were diluted by adding 120 of 100 mM ABC and 880 μL of LC-MS grade water. Protein digestion was conducted as previously mentioned.

Method 3 - (ACN-urea-RapiGest-containing buffer with ISD). Here, 50 μL of 30% ACN, 100 mM ABC, 45 μL of 8 M urea, and 5 μL of 1% RapiGest were added into the samples, and the mixture was incubated for 90 min at 95 °C. Reduction of disulfide bonds was achieved by adding 5.6 μL of 700 mM DTT to the samples and subsequently incubated for 30 min at 37 °C. Alkylation was accomplished by adding 18.4 μL of 700 mM IAA followed by a 30-min incubation at 37 °C in the dark. Samples were diluted by adding 120 of 100 mM ABC and 880 μL of LC-MS grade water. Trypsinization was carried out as already mentioned.

The resulting peptides were desalted on Waters Sep-Pak C18 cartridges (Fisher Scientific, NH, USA). Peptides were desalted using 5% methanol with 0.1% TFA and were subsequently eluted using 50% ACN with 0.1% TFA. Peptide eluates were vacuum dried using a SpeedVac concentrator (Thermo Scientific, MA, USA) and were then stored at −80 °C until LC-MS/MS analysis.

### 2.4. Liquid chromatography-mass spectrometry (LC-MS/MS) analysis

LC-MS/MS analysis was performed using Ultimate 3000 RSLCnano (ThermoFisher Scientific, MA, USA) coupled to Orbitrap Exploris 480 mass spectrometer (ThermoFisher Scientific, MA, USA). The dried peptides were reconstituted in 30 μL of loading buffer (0.08% TFA in 2.5% ACN). Afterward, the peptide concentration was measured using NanoDrop 2000 (Thermo Scientific, MA, USA) absorbance at 280 nm. About 800 ng of peptides for each sample were injected into the LC system and analyzed in 3 technical replicates. First, peptides were trapped and concentrated on an Acclaim™ PepMap™ 100C18 trap column (ThermoFisher Scientific, MA, USA) of 300 μm i.d x 5 mm, and packed with 5 μm, 100 Å particles. Subsequently, 75 μm i.d x 15 cm Acclaim™ PepMap™ RSLC 100 reverse phase C18 analytical column packed with 2 μm particles having 100 Å pore size, was used to separate peptides at a flow rate of 300 nL/min. Analytical column was first equilibrated for 10 min at 2.5% solvent B (0.1% (v/v) TFA in acetonitrile) and 97.5% of solvent A (0.1% (v/v) TFA in water). Following, to separate the peptides, solvent B was increased in a 90-min gradient between 2.5% and 40%. A post-gradient cycle of 99% B was followed by a post-run equilibration at 2.5% B. The analytical column was coupled to the Nanospray Flex Ion Source. Recording of all MS measurements and spectra was done in resolution positive ion mode with a high voltage of 2500 V. For DDA mode, the ion transfer tube was heated to a temperature of 250 °C. MS1 data was acquired by setting the Orbitrap resolution to 120000, an MS scan range of 350−1200 $m/z$, an AGC (automatic gain control) level to custom mode, and a maximum injection time mode to auto. Precursor ions with charges between +2 and +6 and intensity values over 5.0e3 were selected for subsequent higher-energy C-trap dissociation (HCD) fragmentation and MS2 scanning. Precursors were isolated with an $m/z$ window of 2 and fragmented by HCD set at 30%. The product/fragment ions were channeled to the Orbitrap for the MS2 acquisition at a scan resolution of 15000 and a maximum injection time mode set to 60 ms. Repeated sampling was avoided by setting the dynamic exclusion mode to custom, exclusion after n times to 1, exclusion duration to 20, mass tolerance to 10 parts per million (ppm). For data-independent acquisition (DIA) mode, precursor mass range was 400−1100, isolation window ($m/z$) of 8, window overlap ($m/z$) of 1, number of scan events set 87, collision energy of 30% and in a fixed mode, orbitrap resolution of 15000, and the scan range mode was set to auto. In addition, the AGC target was set to custom mode, the maximum injection time set to 25 ms, and microscan was set to 1.

### 2.5. MS data analysis

Mass spectrometer DDA data were processed with MaxQuant [32] (v1.6.17.0). A reviewed UniProt human proteome database with 20381 protein entries (download on March 4, 2021) was used. MaxQuant data processing was done as previously described [33], with a few modifications. The fixed modification was set to carbamidomethylation of cysteines and the false discovery rate (FDR) for both protein and peptide-to-spectrum matches (PSM) levels set at 0.01. A spectral library was generated from DDA-MS data using the FragPipe (v14.0) workflow that comprises MSFragger [34] (v3.1.1), Philosopher (v3.4.13), and Python (3.8.5). The generated library consisted of 2058 protein isoforms, 2058 protein groups, and 17001 precursors in 14702 elution groups. DIA-MS RAW files were processed with Data-Independent Acquisition by Neural

Networks (DIA-NN) software (v1.7.15) [35]. DIA-NN was operated in both library and library-free modes. The gene-centric output matrix was used for further analysis in an R statistical environment (v4.1.0). Protein intensities values for the processed DDA and DIA data were normalized by the median method followed by logarithmic (base 10) transformation. Custom R scripts were used for creating visualizations of the processed data.

### 2.6. Data availability

The mass spectrometry proteomics data have been deposited to the ProteomeXchange Consortium via the PRIDE [36] partner repository with the data set identifier PXD029497.

## 3. Results

### 3.1. Comparative evaluation of different lysis buffer compositions

To establish a robust, simple, and precise FFPE tissue DIA-MS proteomics workflow, we first evaluated the efficiency of three ISD-based protocols (Method 1, Method 2, and Method 3) for protein extraction and digestion. Firstly, lysis buffers were used to analyze the samples of GBM FFPE tissue sections of varying thicknesses (4 μm, 10 μm, and 15 μm) using DDA-MS (Fig. 1).

The number of identified proteins was compared between the methods and the results are shown in Supplementary Fig. 1a. All the methods showed to be sensitive enough to detect more than 1000 proteins from 4 μm tissue microdissection. More specifically, with

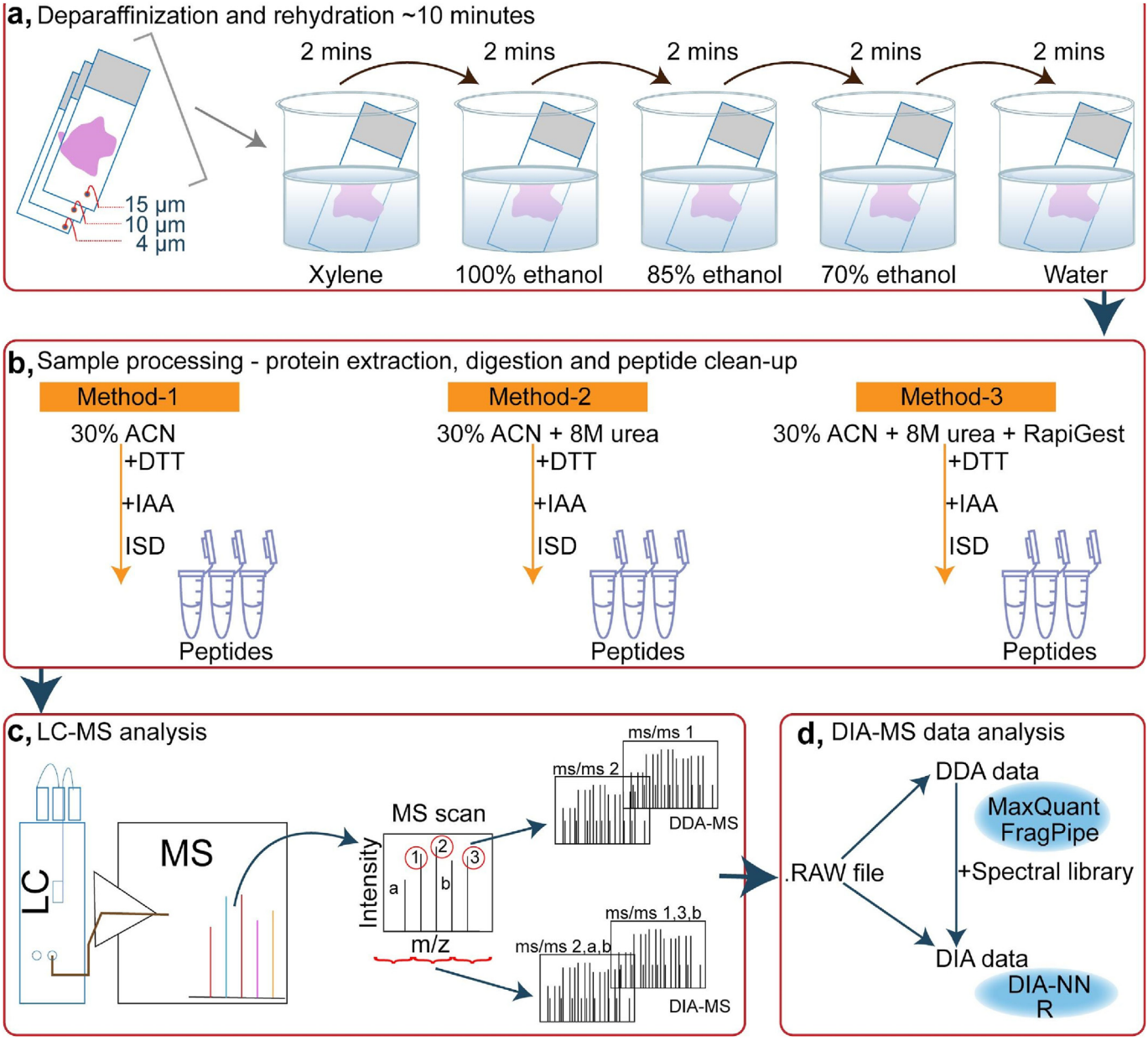


**Fig. 1.** Method evaluation and DIA-MS analysis of GBM FFPE tissues workflow. a, Deparaffinization and rehydration of FFPE tissue sections. The 4 μm, 10 μm, or 15 μm thick GBM tissue sections were first deparaffinized by two xylene washes followed by rehydration using a gradient of ethanol washes (100%, 85%, and 70%) and a final wash with LC-MS grade water. b, Protein extraction, digestion, and peptides clean-up. Tissues were scrapped into the Eppendorf tubes and three methods were each applied to process the deparaffinized and rehydrated tissue sections. c, LC-MS analysis of the resulting peptides were analyzed by Ultimate 3000 RSLCnano coupled to Orbitrap Exploris 480 mass spectrometer. d, DIA-MS data analysis using DIA-NN with MSFragger-generated spectral library.

Method 1, Method 2, and Method 3, we have detected 1274 ± 159, 1405 ± 15, and 1311 ± 171 proteins, respectively (results are shown as mean ± standard deviation [SD]). Moreover, we observed a trend showing urea-containing buffers had higher numbers of protein identifications than the ACN only buffer, which agrees with our previous study on FF uterus tissue [37]. For 10 μm thick sections, 1356 ± 38, 1303 ± 75 and 1347 ± 6 proteins were identified by Method 1, Method 2, and Method 3, respectively. A similar trend was witnessed with 15 μm thick sections. The average number of detected proteins by all methods for 4 μm (1330 ± 68) thick tissue was comparable to 10 μm (1335 ± 28) or 15 μm (1337 ± 10) thick sections implying that small tissue thickness as 4 μm can be used. However, a somewhat higher SD value for 4 μm tissue compared to 10 μm and 15 μm tissue microdissections might be related to the decreasing amounts of input material for ISD proteomic analysis [37]. In our further work, we focused on protein quantification from DDA measurements, and results showed that slightly less than 1000 proteins on average in any of the measurement groups were quantified (Supplementary Fig. 1b).

Next, we overlapped proteins identified by individual methods for all tissue thicknesses to determine the proportion of common proteins. Results from 3 technical replicates were first combined and unique IDs in each group were overlapped. A high percentage (>90%) overlap was observed with 4 μm, 10 μm, and 15 μm reporting, 91%, 95%, and 95% of shared proteins, respectively (Supplementary Fig. 1c). This demonstrates that almost all the detected proteins in each case were similar, indicating a similarity in the performance of tested methods. Consequently, the high percentage of shared proteins among the methods has shown a similar distribution pattern for gene ontology (GO) terms and physicochemical characteristics of the identified proteins (Supplementary Fig. 1d). Further, we selected a few (20) GO terms previously shown to have differential regulation in GBM [38,39]. The highest percentage of the top five cellular components are cytosolic, followed by the extracellular exosome, cytoplasmic, nuclear, and plasma membrane. As illustrated in the inset in Supplementary Fig. 1d, a median molecular weight (MW) of ~42 kDa was observed across the comparison groups. Further, in the evaluation of misscleaved sites, methods showed similarity in the number of missed cleavages, and over 60% of cleavage sites were fully cleaved in all the comparison groups (Supplementary Fig. 2). Overall, Method 3 (25.1%) showed a slightly smaller proportion of missed cleavages relative to Method 1 (25.3%) and Method 2 (27.5%) — indicating a beneficial effect of including RapiGest.

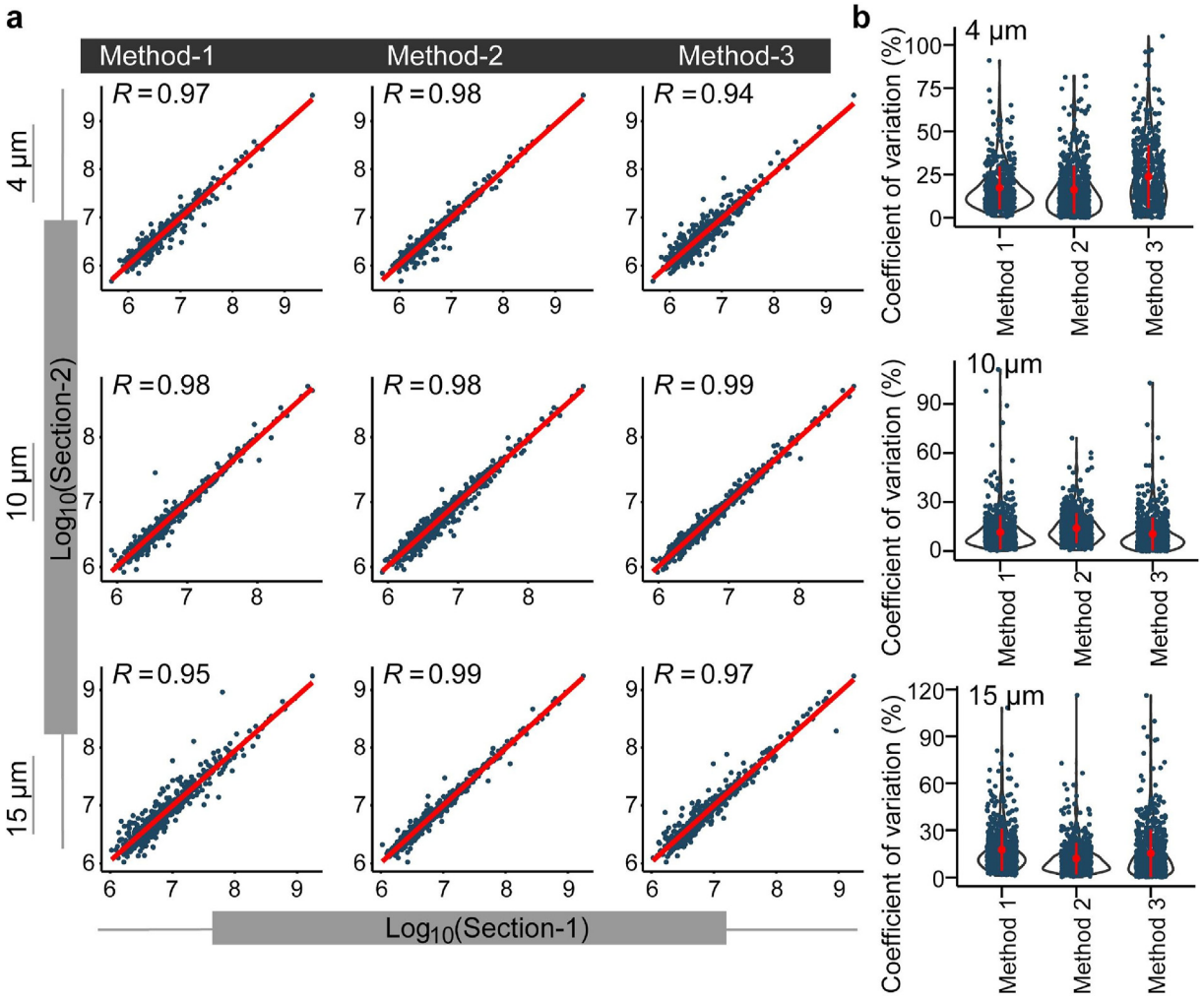


**Fig. 2.** Quantitative reproducibility assessment. a, Scatter plots illustrating the correlation between technical replicates processed by each of the three methods. The LFQ values were normalized using the quantile method, and then log (base 10) transformed. Each dot in the plot represents a protein, and the red line indicates the regression line. The Pearson's correlation coefficient value is indicated by *R*. Each column displays the scatter plot for the individual method e.g., from left-to-right: Method 1, Method 2, and Method 3. Each row displays the scatter plot for different sizes of tissue sections e.g., from top-to-bottom: 4 μm, 10 μm, and 15 μm. b, Violin plots showing CV for each method using different tissue sizes. (For interpretation of the references to color in this figure legend, the reader is referred to the Web version of this article.)

### 3.2. Quantitative analysis and evaluation of precision

Quantitative analysis is an important aspect of biomarker discovery and presents a particular analytical challenge in DDA strategies due to missing intensities values. Thus, we focused on evaluating the precision of quantification methods in each tissue thickness category. The data was quantile-normalized before performing logarithmic transformation (base 10). We correlated technical replicates using a pairwise Pearson's correlation coefficient to determine quantitative reproducibility between sections processed with the same method. We observed a high Pearson's correlation ($R > 0.90$) between technical replicates in all the methods (Fig. 2a). We subsequently carried out a coefficient of variation (CV) analysis to discern methods that allowed minimal fluctuations in protein quantification. CV analysis was applied to the log-transformed data and the resulting values were expressed as percentages. From this, we noticed less variability in protein quantification in almost all the methods as we could observe CV values of <20% (Fig. 2b). For 4 μm thick sections, we could observe 17.3%, 16.2%, and 23.8% CV values in Method 1, Method 2, and Method 3, respectively. In 10 μm thick sections, 11.5%, 14.0% and 10.5% CVs corresponded to Method 1, Method 2 and Method 3. As for the 15 μm thick sections, we found 17.5%, 12.0%, and 15.3% with Method 1, Method 2, and Method 3, respectively. High precision was witnessed with Method 2 and 3 where 10 μm or 15 μm thick sections were used. We then calculated the mean CVs in each thickness category by summing up CVs for the three methods and averaging. Overall, the 4 μm thick sections comparatively reported the highest variation with a mean CV of 19.1%, which is likely to be related to the low input material. Mean CV values of 12% and 14.9% were recorded for 10 μm and 15 μm thick sections, respectively.

### 3.3. Comparison of sequence coverage

Sequence coverage represents the average percentage of amino acids covered in the identified protein. The type of strategy applied to prepare samples for mass spectrometric proteomic analysis can influence the sequence coverage of the identified proteins [40]. We compared the sequence coverage as a function of protein abundance for the covered proteome by each method (Fig. 3a). The sequence coverage and intensity values for technical replicates analyzed by the same method were averaged to obtain mean values. In 4 μm sections, all methods performed similarly in terms of sequence coverage of the proteins (Method 1 = 14.3%, Method 2 = 14.1% and Method 3 = 14.8%). We, however, observed an increasing trend in the percentage sequence coverage in the case of 10 μm and 15 μm thick tissue compared to 4 μm thick sections. For 10 μm thick sections, the coverage values were 18.4%, 16.5%, and 17.5% for Method 1, Method 2, and Method 3, respectively. On the other hand, the 15 μm thick tissue sections reported the following coverage values; 17.5%, 18.4%, and 17.9% for Method 1, Method 2, and Method 3, respectively. The difference in the sequence coverage between relatively smaller sections (4 μm) and larger (10 μm or 15 μm) is likely attributable to the amounts of the input material. Interestingly, this suggestion was perfectly demonstrated with the urea-RapiGest-containing buffer (Method 3) as we could see an increase in the percentage of sequence coverage with 14.8%, 17.5%, 17.9% reported for 4 μm, 10 μm and 15 μm thick sections, respectively. Next, we were interested in comparing the number of proteins having percentage sequence coverage greater than 20%. From this comparison, we could observe that Method 2 and Method 3 showed the number of proteins having a sequence coverage greater than 20% increase with increasing tissue size from 4 μm to 15 μm.

For the three thickness categories, we examined them based on proteins relevant to GBM that were covered. At first, we cataloged most proteins that have been reported as clinically relevant or candidate biomarkers for GBM (Supplementary Table 1). The raw (LFQ intensities) protein abundance values were quantile-normalized and subsequently, log (base 10) transformed, and the outputs were ranked. Finally, the ranked lists were intersected with the list containing GBM-relevant proteins. We noticed an increase in the number of GBM-relevant proteins with increasing tissue thickness, e.g., 72, 86, and 91 for 4 μm, 10 μm, and 15 μm, respectively (Fig. 3b).

Having performed a comparative evaluation of the three methods, we selected Method 3 (ACN-urea-RapiGest-containing buffer) and applied it to analyze five patient samples. Even though all the methods demonstrated comparable performance we could witness some consistency in protein identification and quantification with Method 3, which informed the decision to select it for the next step in our DIA-MS analysis workflow.

### 3.4. DIA-MS reliably detects and quantifies putative GBM biomarkers in FFPE tumor tissues

We optimized a DIA-MS workflow with an 8 Da window to perform an in-depth analysis of FFPE tissues to capture and quantify GBM-relevant proteins. Patient-derived GBM tissue samples (n = 5) with 15 μm thick sections were processed in three biological replicates using Method 3 (ACN-urea-RapiGest-containing buffer). With our single-shot DIA-MS workflow, we were able to identify >1700 proteins across the samples. This was a huge improvement in proteome coverage compared to what we observed with the DDA analysis workflow (Fig. 4a). We compared different functionalities of DIA-NN by analyzing the data in either library-free or spectral library mode (Supplementary Fig. 3a and b; Supplementary Fig. 4a, b, c, d). We also compared DDA-MS and DIA-MS based on the sequence coverage. DIA-MS achieved a higher mean sequence coverage of 28.6% than 24.7% by DDA-MS (Supplementary Fig. 5a, b, c). DIA-MS has been demonstrated in several studies [10,41–43] to outperform DDA-MS in terms of sensitivity and proteome coverage. Therefore, this result corroborates such earlier findings. To interrogate the protein expression profile, we proceeded with the gene-centric matrix output of DIA-NN. Using protein intensities, we performed Pearson's cross-correlations of all LC-MS runs (n = 15) and technical replicate values were first averaged before correlating the samples. The global correlation matrix revealed strong agreement among replicates of the sample with a high Pearson's correlation coefficient of R > 0.8 (Supplementary Fig. 6). Further, we explored the CV for all quantified proteins in each patient sample. All the samples recorded low median CV values of <20%, with an average of 16.2% and a median of 11.9% (Fig. 4b). The low CV values indicate the high precision of our DIA-MS workflow for in-depth protein quantification. To explore the differences in the patient proteome profiles, we performed a principal component analysis (PCA) of quantified proteins (n = 1498) in all samples.

The PCA clearly classified the samples according to the patient where they were derived (Fig. 4c). This finding demonstrates that the separation is driven by patient-specific proteome signatures. We further examined the expression values of proteins across samples. First, a mean intensity value was calculated and then ranked from highest to lowest. A screen of the top twenty proteins in terms of intensity values revealed the presence of GBM-relevant markers such as glial fibrillary acidic protein (GFAP) [44–46] (Fig. 4d). Similarly, VIM and MBP, which showed high-intensity values relative to other proteins, have been reported as valuable biomarkers in GBM [47,48]. The confirmation of the presence of the proteins unique to glioma- and specifically GBM in the analyzed data demonstrates our DIA-MS workflow's high sensitivity and robustness in detecting and quantifying disease-relevant proteins (e.g., FN1 and BASP1). Next, we set out to explore the variation in

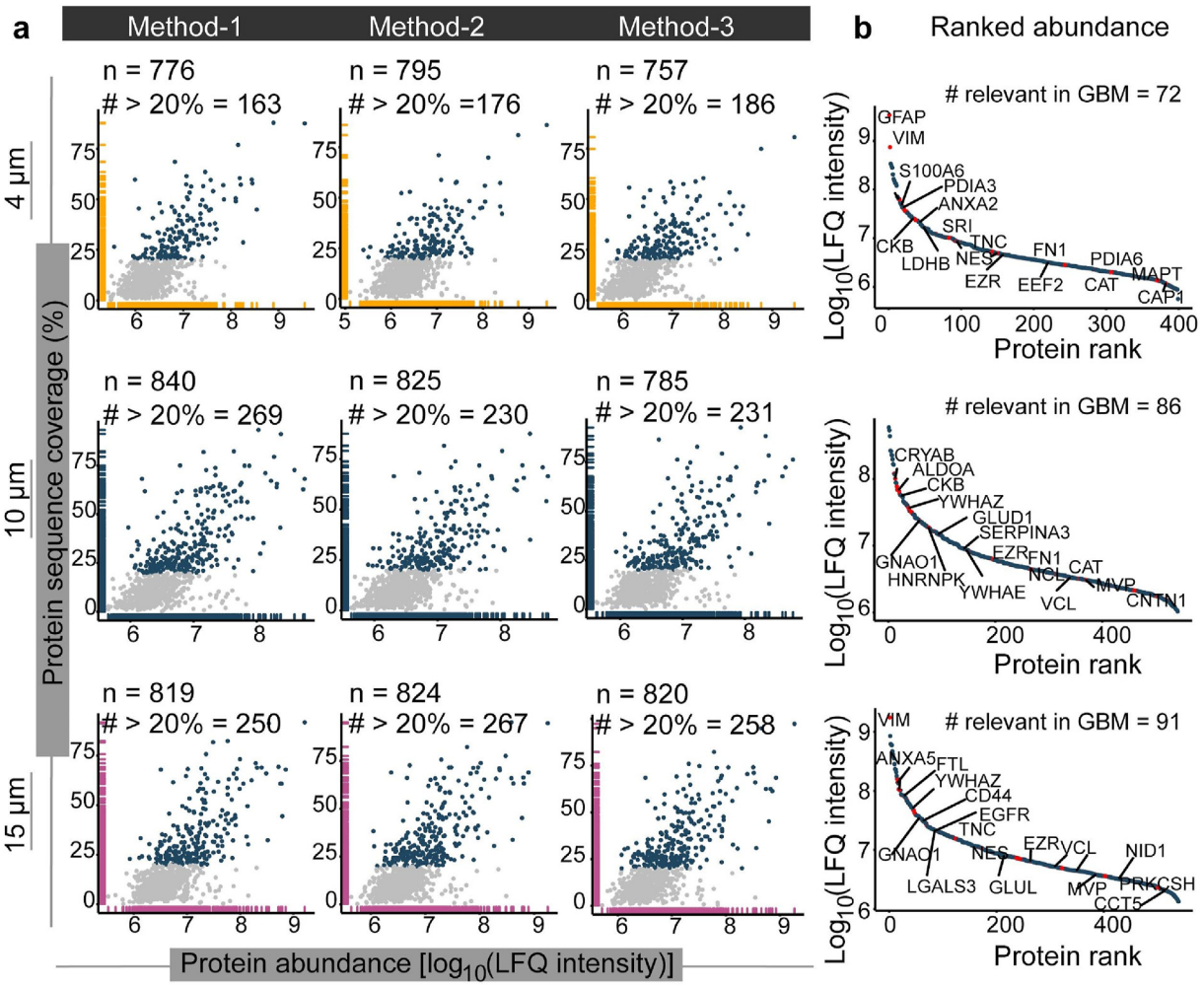


**Fig. 3.** Sequence coverage and ranked abundance across the methods. a, Scatter plots of the percent of mean protein sequence coverage (y-axis) and quantile-normalized and logarithmically (base 10) transformed mean LFQ values (x-axis). Each column represents the method type (Method 1, Method 2, and Method 3 successively) and each row represents the size of the tissue section (4 µm, 10 µm, and 15 µm successively). Median protein sequence coverage averaged at 20%, and thus, proteins detected with sequence coverage above this value were considered highly covered by peptides. The gray color indicates proteins with sequence coverage less or equal to 20% while cello color indicates proteins with sequence coverage above 20%. A density trace marked with a rug on both axes shows the spread of values along the coordinates, and the color codes of the rug correspond to the different tissue sizes. The number of complete observations in all replicates for each scatter is shown by n. The number of proteins with sequence coverage greater than 20% is shown by the # symbol. b, Dynamic range plot based on quantile normalized and logarithmically (base 10) transformed mean LFQ values of consistently identified proteins in all methods for each size of tissue section (4 µm from top, 10 µm middle and 15 µm bottom) used. The x-axis shows the ranked order distribution. The red color indicates proteins that have been reported as potential biomarkers in GBM. (For interpretation of the references to color in this figure legend, the reader is referred to the Web version of this article.)

quantifying top twenty proteins based on intensity values by calculating their CVs using mean expression intensities. The CV analysis recorded low values of 11.4% and 10.5% for mean and median, respectively (Supplementary Fig. 7). This result further supports the robustness of our pipeline for protein quantification.

In order to investigate the observed proteome differences in the PCA (Fig. 4c) further, we performed an unsupervised hierarchical clustering on the relative expression levels of 78 proteins with promising clinical utility (Supplementary Table 1) in the context of GBM. As illustrated in Fig. 5a, each patient displayed a distinct gradient on the heatmap, concordance with the PCA result. Next, we selected a few clusters of proteins focusing on those having high relative expression levels and determined the variation in quantification. CV was calculated for replicates of the proteins for each cluster. We observed a lower CV at the cluster level (Fig. 5a) compared to the global CV witnessed in Supplementary Fig. 7. Again, all this data supports the robustness of the pipeline that we used in this analysis. Next, we leveraged STRING software to query the nature of the interaction of the 78 GBM-relevant proteins (Fig. 5b). The network reported significant interactions with protein-protein interaction (PPI) enrichment p-value of <1.0e-16 and an average local clustering coefficient of 0.527. This result demonstrates the ability of the DIA-MS workflow in this study to capture the PPI of interest that could be interrogated further to get some exciting biological insights concerning GBM tumor evolution and progression.

### 3.5. Screening of immune-related genes in a DIA-MS dataset

With the intensified interest in developing novel immunotherapeutics, a comprehensive understanding of how immune cells infiltrate GBM is necessary. We screened our DIA-MS dataset to identify the detected immune-related genes. Out of the 1498 quantified proteins, 348 were associated with the immune system (Supplementary Data 1, Supplementary Table 2). Next, we leveraged the recently published CPTAC (Clinical Proteomic Tumor Analysis Consortium) mRNA data [49] to correlate with the protein expression levels in our dataset. When we intersected the CPTAC mRNA dataset with the cataloged 348 genes, we found 320 common immune-related genes. A low positive Pearson's correlation

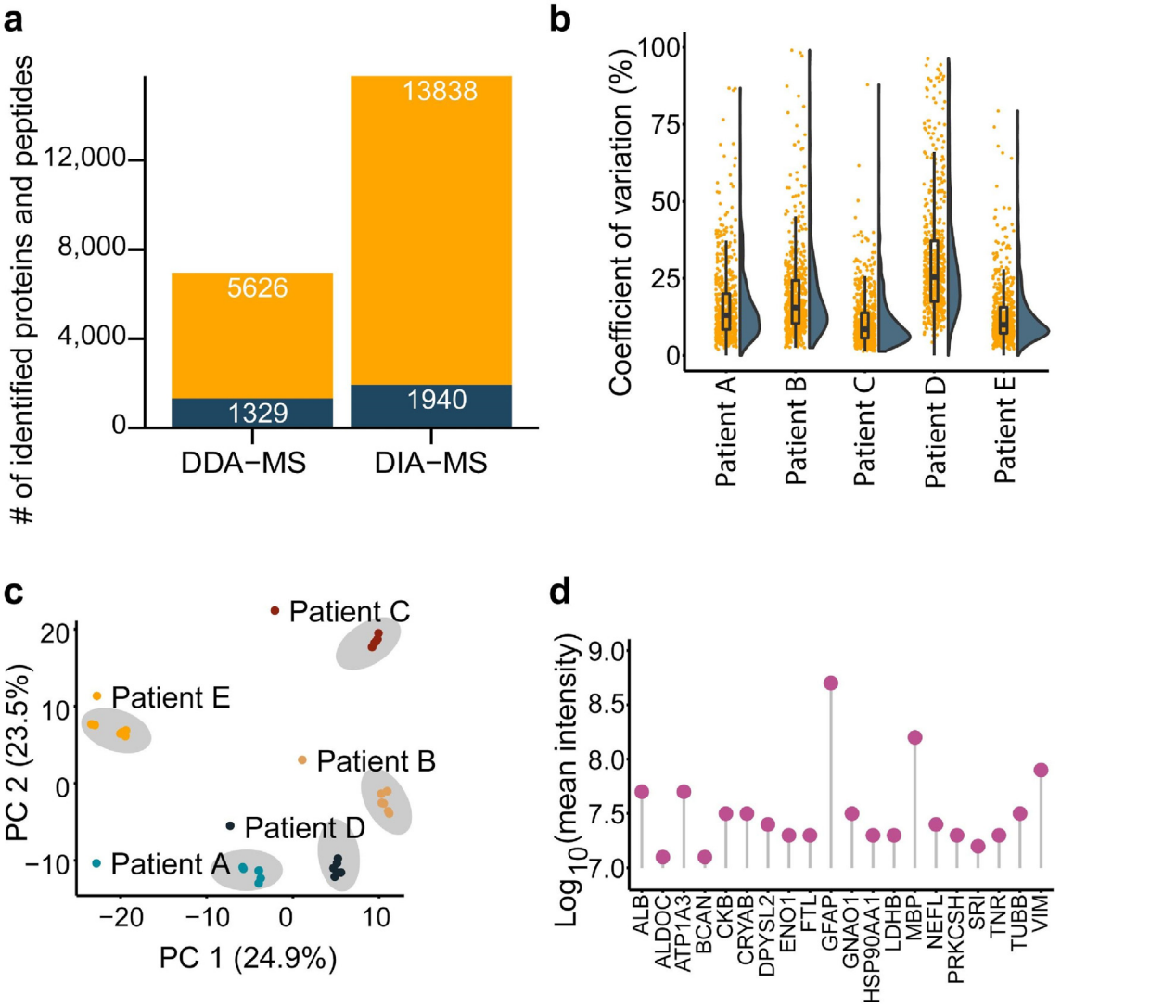


**Fig. 4.** DIA-MS analysis of FFPE tissues derived from GBM patients (n = 5). a, Bar plots displaying the number of identified peptides and proteins with either DDA-MS or DIA-MS. b, Raincloud plot illustrates the CV of quantile-normalized protein intensities in all the sections for each patient e.g., A, B, C, D, and E. The midline of the boxplot in the raincloud plot indicates the median CV, the half violin illustrates the density of values. Each dot in the plot corresponds to the calculated CV for the individual protein in all sections per patient. c, Principal component analysis of proteins detected in all patient FFPE tissue samples. The color corresponds to different patients. d, Lollipop plot showing the top 20 GBM-relevant proteins. The ranking was based on quantile-normalized log (base 10) transformed mean intensity. (For interpretation of the references to color in this figure legend, the reader is referred to the Web version of this article.)

coefficient of $R = 0.37$ (Fig. 6a) was reported when we compared the DIA readouts to CPTAC's mRNA expression levels (FPKM values). A low correlation between transcriptome and proteome has been reported in previous studies [50,51], and this is consistent in our study. The transcripts expression levels do not completely reflect the protein abundance since proteins undergo various post-transcriptional modifications. This phenomenon possibly contributes to the low positive correlation between transcriptome and proteome. A pairwise protein-level correlation between data in this study and CPTAC reported a positive Pearson's correlation coefficient value of $R = 0.42$ (Supplementary Fig. 8). Some of the proteins e.g. MIF, which are currently being pursued as novel drug targets, showed elevated relative expression levels (Fig. 6b).

## 4. Discussion

FFPE tissue samples have shown superiority over other sample types since they are stable over long storage; hence, providing more opportunities for researchers to discover clinically-relevant proteins [15]. Thus, efficient protein extraction from FFPE samples is crucial for targeted and discovery-based proteomics research. Presently, several methods applying DDA-MS for FFPE tissue sample proteomics analysis have been reported [52–54]. DIA-MS is increasingly being applied in tissue proteomics. However, there are currently few studies on GBM where DIA-MS has been performed. Therefore, we aimed to establish a simple and highly precise DIA-MS workflow able to detect and quantify both GBM-relevant and immune-related proteins in the GBM tumor.

The analytical superiority of DIA-MS over DDA-MS has been demonstrated in several studies [3,43]. Besides, it was recently shown that DIA-MS could yield results comparable to those generated using selected reaction monitoring (SRM) [10]. Our study's observed increment in the number of detected proteins with DIA-MS relative to DDA-MS was consistent with earlier works [55]. The random sampling of the most abundant ion species in the DDA-MS has been cited as one of the contributing factors in lower

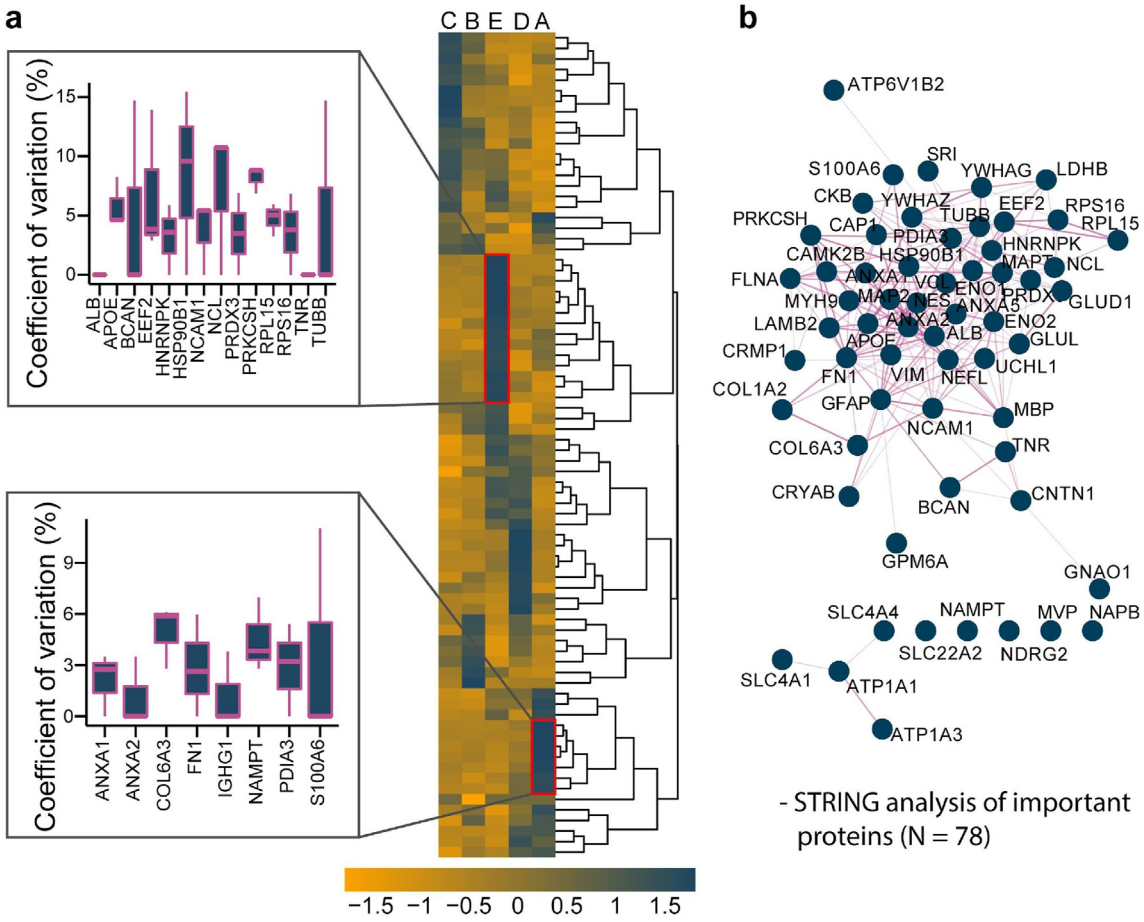


**Fig. 5.** Heatmap and STRING diagram for a few selected proteins. a, Heatmap of relative expression levels of all proteins detected in all DIA-MS runs. Unsupervised hierarchical clustering is based on the scaled protein expression values. Clusters with high expression values are marked with cello color while those with low expression values are indicated with orange color. The boxplots show the CV distribution for proteins in the selected clusters. b, STRING diagram displaying the interaction of the 78 GBM-relevant proteins. (For interpretation of the references to color in this figure legend, the reader is referred to the Web version of this article.)

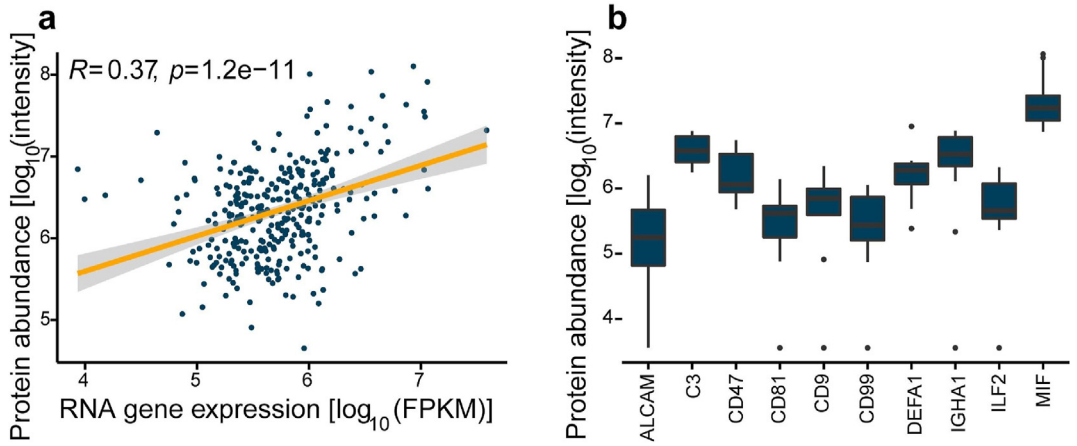


**Fig. 6.** Exploring expression levels of immune-related genes. a, Scatter plot showing the correlation between protein and mRNA expression levels. The yellow line represents the line of best fit with the shaded area showing the 95% confidence interval. R and p-value are based on Pearson's coefficient correlation. b, Boxplot showing the abundance of top immune-relevant proteins. (For interpretation of the references to color in this figure legend, the reader is referred to the Web version of this article.)

protein identification in comparison to DIA-MS. Moreover, the stochastic sampling nature in DDA-MS often generates a high number of missing protein intensity values [3]. We achieved high precision in protein quantification, indicated by the low CV values.

The DIA-MS detected most of the proteins relevant to GBM pathology, including FN1, VIM, MBP, and GFAP [56–60]. VIM and GFAP are co-expressed in human glioma [61], and overexpression of VIM has been associated with poor survival outcomes for GBM patients [62]. The co-expression of these two proteins is evident in our DIA-MS data, as depicted by their relatively elevated expression

intensity values (Fig. 4d). Taken together, this evidence is a demonstration of how sensitive and precise this DIA-MS workflow is for the quantification of proteins in FFPE tissue samples. The detection of these proteins in glioma samples has been performed mainly by using relatively less sensitive techniques. A recent study using a Q-Exactive mass spectrometer reported a significant elevation of VIM in GBM patient specimens [56].

Overexpression of brain acid soluble protein 1 (BASP1) has been shown to promote the proliferation of cancer cells [63]. In pancreatic cancer tissue, quantitative proteomics analysis using Q Exactive Plus Hybrid Quadrupole-Orbitrap mass spectrometer identified BASP1 as a candidate prognostic biomarker [64]. BASP1 plays a role in the organization of the cytoskeleton elements. FN1, a glycoprotein with cell adhesive features, has been implicated in tumor cell migration and invasion by interacting with integrin proteins [65]. Additionally, its overexpression in glial tumors has been associated with an increased migration rate of tumor cells [66]. Some of the immune-related proteins (e.g., MIF, CD47, and TTYH1) that we detected and quantified with high precision are currently being interrogated as potential targets for immune-based therapy. MIF has been found differentially expressed in a subpopulation of GBM myeloid-derived suppressor cells and could be potentially targeted to repress immunosuppression in tumor microenvironment [67]. Elevated expression of MIF with poor survival was recently reported in GBM samples in patients with O-6-Methylguanine-DNA Methyltransferase (MGMT) methylation [68].

To conclude, the quantitative MS proteomics field is quickly gravitating towards simple and highly sensitive workflows that enable in-depth coverage and precise quantification of proteome-wide expression. In this regard, DIA-MS has emerged top and is increasingly being applied to quantify proteins in tissues. Therefore, accurate and precise quantification of proteins in patient-derived FFPE samples is expected to provide new leads to discover novel therapeutic targets. In this study, a simple DIA-MS workflow was established and was successfully applied to patient-derived GBM tissue samples (n = 5). This DIA-MS approach enabled precise detection and quantification of proteins, and over 1400 proteins were quantified. Importantly, immune-related (e.g. MIF) and GBM-relevant proteins (e.g., GFAP) were detected and quantified. Finally, we anticipate that our approach would be useful for researchers interested in quantitative MS proteomic analysis of FFPE tissue specimens. Notably, it facilitates the detection and quantification of protein candidates for new therapeutic strategies for glioma and other malignant tumors.

## Funding

This research was funded by the International Research Agenda's Program of the Foundation for Polish Science (MAB/2017/03) (K.W, J.F, N.U, D.R.G, T.R.H, S.K, I.D).

## CRediT authorship contribution statement

**Kenneth Weke:** Conceptualization, Formal analysis, Investigation, Visualization, Writing – original draft, Software, Writing – review & editing. **Sachin Kote:** Conceptualization, Methodology, Investigation, Supervision, Project administration, Writing – review & editing. **Jakub Faktor:** Formal analysis, Investigation, Writing – review & editing. **Sofian Al Shboul:** Resources, Investigation, Writing – review & editing. **Naomi Uwugiaren:** Conceptualization, Methodology, Writing – review & editing. **Paul M. Brennan:** Resources, Investigation, Writing – review & editing. **David R. Goodlett:** Conceptualization, Methodology, Writing – review & editing. **Ted R. Hupp:** Conceptualization, Methodology, Funding acquisition, Writing – review & editing. **Irena Dapic:** Conceptualization, Methodology, Supervision, Project administration, Writing – review & editing, . All authors read and approved the paper.

## Declaration of competing interest

The authors declare that they have no known competing financial interests or personal relationships that could have appeared to influence the work reported in this paper.

## Acknowledgments

This study was funded by the International Research Agenda's Program of the Foundation for Polish Science (MAB/2017/03) (K.W, J.F, N.U, D.R.G, T.R.H, S.K, I.D). The “International Centre for Cancer Vaccine Science” project is carried out within the International Research Agendas programme of the Foundation for Polish Science co-financed by the European Union under the European Regional Development Fund. The authors would also like to thank the CI-TASK, Gdansk, and the PL-Grid Infrastructure, Poland for providing their hardware and software resources.

We are grateful for funding for technology development and platform support for The Pan-Canadian Proteomics Centre (PCPC), from Genome Canada, and Genome British Columbia through the Genomics Technology Platform (GTP) program for operations and technology development (264PRO) (D.R.G).

We are grateful to the NHS Lothian Bioresource for facilitating the collection of tissue used in this study (P.M.B).

## Appendix A. Supplementary data

Supplementary data related to this article can be found at https://doi.org/10.1016/j.aca.2022.339695.

## References

[1] M. van Oostrum, B. Campbell, C. Seng, M. Müller, S. tom Dieck, J. Hammer, P.G.A. Pedrioli, C. Földy, S.K. Tyagarajan, B. Wollscheid, Surfaceome dynamics reveal proteostasis-independent reorganization of neuronal surface proteins during development and synaptic plasticity, Nat. Commun. 11 (2020) 4990, https://doi.org/10.1038/s41467-020-18494-6.

[2] K.W. Li, M.A. Gonzalez-Lozano, F. Koopmans, A.B. Smit, Recent developments in data independent acquisition (DIA) mass spectrometry: application of quantitative analysis of the brain proteome, Front. Mol. Neurosci. 13 (2020) 248, https://doi.org/10.3389/fnmol.2020.564446.

[3] L. Krasny, P.H. Huang, Data-independent acquisition mass spectrometry (DIA-MS) for proteomic applications in oncology, Mol. Omics 17 (2021) 29–42, https://doi.org/10.1039/D0MO00072H.

[4] G. Hou, X. Lou, Y. Sun, S. Xu, J. Zi, Q. Wang, B. Zhou, B. Han, L. Wu, X. Zhao, L. Lin, S. Liu, Biomarker discovery and verification of esophageal squamous cell carcinoma using integration of SWATH/MRM, J. Proteome Res. 14 (2015) 3793–3803, https://doi.org/10.1021/acs.jproteome.5b00438.

[5] Y. Liu, R. Hüttenhain, S. Surinova, L.C. Gillet, J. Mouritsen, R. Brunner, P. Navarro, R. Aebersold, Quantitative measurements of N-linked glycoproteins in human plasma by SWATH-MS, Proteomics 13 (2013) 1247–1256, https://doi.org/10.1002/pmic.201200417.

[6] C. Ludwig, L. Gillet, G. Rosenberger, S. Amon, B.C. Collins, R. Aebersold, Data-independent acquisition-based SWATH-MS for quantitative proteomics: a tutorial, Mol. Syst. Biol. 14 (2018), e8126, https://doi.org/10.15252/msb.20178126.

[7] F. Zhang, W. Ge, G. Ruan, X. Cai, T. Guo, Data-independent acquisition mass spectrometry-based proteomics and software tools: a glimpse in 2020, Proteomics 20 (2020), 1900276, https://doi.org/10.1002/pmic.201900276.

[8] B.C. Collins, C.L. Hunter, Y. Liu, B. Schilling, G. Rosenberger, S.L. Bader, D.W. Chan, B.W. Gibson, A.-C. Gingras, J.M. Held, M. Hirayama-Kurogi, G. Hou, C. Krisp, B. Larsen, L. Lin, S. Liu, M.P. Molloy, R.L. Moritz, S. Ohtsuki, R. Schlapbach, N. Selevsek, S.N. Thomas, S.-C. Tzeng, H. Zhang, R. Aebersold, Multi-laboratory assessment of reproducibility, qualitative and quantitative performance of SWATH-mass spectrometry, Nat. Commun. 8 (2017) 291, https://doi.org/10.1038/s41467-017-00249-5.

[9] P. Bouchal, O.T. Schubert, J. Faktor, L. Capkova, H. Imrichova, K. Zoufalova, V. Paralova, R. Hrstka, Y. Liu, H.A. Ebhardt, E. Budinska, R. Nenutil,

R. Aebersold, Breast cancer classification based on proteotypes obtained by SWATH mass spectrometry, Cell Rep 28 (2019) 832–843, https://doi.org/10.1016/j.celrep.2019.06.046, e7.
[10] Y.J. Kim, S.M.M. Sweet, J.D. Egertson, A.J. Sedgewick, S. Woo, W. Liao, G.E. Merrihew, B.C. Searle, C. Vaske, R. Heaton, M.J. MacCoss, T. Hembrough, Data-independent acquisition mass spectrometry to quantify protein levels in FFPE tumor biopsies for molecular diagnostics, J. Proteome Res. 18 (2019) 426–435, https://doi.org/10.1021/acs.jproteome.8b00699.
[11] P. Steffen, J. Li, J. Chandra, M.S. Ahadi, A.J. Gill, A.F. Engel, M.P. Molloy, Molecular features of lymph node metastasis in T1/2 colorectal cancer from formalin-fixed paraffin-embedded archival specimens, J. Proteome Res. 20 (2021) 1304–1312, https://doi.org/10.1021/acs.jproteome.0c00693.
[12] Y. Gao, X. Wang, Z. Sang, Z. Li, F. Liu, J. Mao, D. Yan, Y. Zhao, H. Wang, P. Li, X. Ying, X. Zhang, K. He, H. Wang, Quantitative proteomics by SWATH-MS reveals sophisticated metabolic reprogramming in hepatocellular carcinoma tissues, Sci. Rep. 7 (2017) 45913, https://doi.org/10.1038/srep45913.
[13] D.M. Marchione, I. Ilieva, K. Devins, D. Sharpe, D.J. Pappin, B.A. Garcia, J.P. Wilson, J.B. Wojcik, HYPERsol: high-quality data from archival FFPE tissue for clinical proteomics, J. Proteome Res. 19 (2020) 973–983, https://doi.org/10.1021/acs.jproteome.9b00686.
[14] Y. Newton, A.J. Sedgewick, L. Cisneros, J. Golovato, M. Johnson, C.W. Szeto, S. Rabizadeh, J.Z. Sanborn, S.C. Benz, C. Vaske, Large scale, robust, and accurate whole transcriptome profiling from clinical formalin-fixed paraffin-embedded samples, Sci. Rep. 10 (2020) 17597, https://doi.org/10.1038/s41598-020-74483-1.
[15] Y. Zhu, T. Weiss, Q. Zhang, R. Sun, B. Wang, X. Yi, Z. Wu, H. Gao, X. Cai, G. Ruan, T. Zhu, C. Xu, S. Lou, X. Yu, L. Gillet, P. Blattmann, K. Saba, C.D. Fankhauser, M.B. Schmid, D. Rutishauser, J. Ljubicic, A. Christiansen, C. Fritz, N.J. Rupp, C. Poyet, E. Rushing, M. Weller, P. Roth, E. Haralambieva, S. Hofer, C. Chen, W. Jochum, X. Gao, X. Teng, L. Chen, Q. Zhong, P.J. Wild, R. Aebersold, T. Guo, High-throughput proteomic analysis of FFPE tissue samples facilitates tumor stratification, Mol. Oncol. 13 (2019) 2305–2328, https://doi.org/10.1002/1878-0261.12570.
[16] S.R. Shi, M.E. Key, K.L. Kalra, Antigen retrieval in formalin-fixed, paraffin-embedded tissues: an enhancement method for immunohistochemical staining based on microwave oven heating of tissue sections, J. Histochem. Cytochem. 39 (1991) 741–748, https://doi.org/10.1177/39.6.1709656.
[17] S. Yamashita, Heat-induced antigen retrieval: mechanisms and application to histochemistry, Prog. Histochem. Cytochem. 41 (2007) 141–200, https://doi.org/10.1016/j.proghi.2006.09.001.
[18] F. Coscia, S. Doll, J.M. Bech, L. Schweizer, A. Mund, E. Lengyel, J. Lindebjerg, G.I. Madsen, J.M. Moreira, M. Mann, A streamlined mass spectrometry–based proteomics workflow for large-scale FFPE tissue analysis, J. Pathol. 251 (2020) 100–112, https://doi.org/10.1002/path.5420.
[19] A. Tanca, M. Abbondio, S. Pisanu, D. Pagnozzi, S. Uzzau, M.F. Addis, Critical comparison of sample preparation strategies for shotgun proteomic analysis of formalin-fixed, paraffin-embedded samples: insights from liver tissue, Clin. Proteonomics 11 (2014) 28, https://doi.org/10.1186/1559-0275-11-28.
[20] M.C. Föll, M. Fahrner, V.O. Oria, M. Kühs, M.L. Biniossek, M. Werner, P. Bronsert, O. Schilling, Reproducible proteomics sample preparation for single FFPE tissue slices using acid-labile surfactant and direct trypsinization, Clin. Proteonomics 15 (2018) 11, https://doi.org/10.1186/s12014-018-9188-y.
[21] A. Pirog, J. Faktor, Z. Urban-Wojciuk, S. Kote, E. Chruściel, Ł. Arcimowicz, N. Marek-Trzonkowska, B. Vojtesek, T.R. Hupp, S. Al Shboul, P.M. Brennan, R.T. Smoleński, D.R. Goodlett, I. Dapic, Comparison of different digestion methods for proteomic analysis of isolated cells and FFPE tissue samples, Talanta 233 (2021), 122568, https://doi.org/10.1016/j.talanta.2021.122568.
[22] J.R. Wiśniewski, P. Ostasiewicz, M. Mann, High recovery FASP applied to the proteomic analysis of microdissected formalin fixed paraffin embedded cancer tissues retrieves known colon cancer markers, J. Proteome Res. 10 (2011) 3040–3049, https://doi.org/10.1021/pr200019m.
[23] J. Nazarian, M. Santi, Y. Hathout, T.J. MacDonald, Protein profiling of formalin fixed paraffin embedded tissue: identification of potential biomarkers for pediatric brainstem glioma, PROTEOMICS, Clin. Appl. 2 (2008) 915–924, https://doi.org/10.1002/prca.200780061.
[24] Y.-Q. Yu, M. Gilar, P.J. Lee, E.S.P. Bouvier, J.C. Gebler, Enzyme-friendly, mass spectrometry-compatible surfactant for in-solution enzymatic digestion of proteins, Anal. Chem. 75 (2003) 6023–6028, https://doi.org/10.1021/ac0346196.
[25] S.A. Luebker, S.A. Koepsell, Optimization of urea based protein extraction from formalin-fixed paraffin-embedded tissue for shotgun proteomics, Int. J. Proteomics 2016 (2016), e4324987, https://doi.org/10.1155/2016/4324987.
[26] A. Alkhas, B.L. Hood, K. Oliver, P. Teng, J. Oliver, D. Mitchell, C.A. Hamilton, G.L. Maxwell, T.P. Conrads, Standardization of a sample preparation and analytical workflow for proteomics of archival endometrial cancer tissue, J. Proteome Res. 10 (2011) 5264–5271, https://doi.org/10.1021/pr2007736.
[27] P. Ostasiewicz, D.F. Zielinska, M. Mann, J.R. Wiśniewski, Proteome, phosphoproteome, and N-glycoproteome are quantitatively preserved in formalin-fixed paraffin-embedded tissue and analyzable by high-resolution mass spectrometry, J. Proteome Res. 9 (2010) 3688–3700, https://doi.org/10.1021/pr100234w.
[28] C.S. Hughes, M.K. McConechy, D.R. Cochrane, T. Nazeran, A.N. Karnezis, D.G. Huntsman, G.B. Morin, Quantitative profiling of single formalin fixed tumour sections: proteomics for translational research, Sci. Rep. 6 (2016) 34949, https://doi.org/10.1038/srep34949.
[29] R. Stupp, W.P. Mason, M.J. van den Bent, M. Weller, B. Fisher, M.J.B. Taphoorn, K. Belanger, A.A. Brandes, C. Marosi, U. Bogdahn, J. Curschmann, R.C. Janzer, S.K. Ludwin, T. Gorlia, A. Allgeier, D. Lacombe, J.G. Cairncross, E. Eisenhauer, R.O. Mirimanoff, Radiotherapy plus concomitant and adjuvant temozolomide for glioblastoma, N. Engl. J. Med. 352 (2005) 987–996, https://doi.org/10.1056/NEJMoa043330.
[30] C.W. Brennan, R.G.W. Verhaak, A. McKenna, B. Campos, H. Noushmehr, S.R. Salama, S. Zheng, D. Chakravarty, J.Z. Sanborn, S.H. Berman, R. Beroukhim, B. Bernard, C.-J. Wu, G. Genovese, I. Shmulevich, J. Barnholtz-Sloan, L. Zou, R. Vegesna, S.A. Shukla, G. Ciriello, W.K. Yung, W. Zhang, C. Sougnez, T. Mikkelsen, K. Aldape, D.D. Bigner, E.G. Van Meir, M. Prados, A. Sloan, K.L. Black, J. Eschbacher, G. Finocchiaro, W. Friedman, D.W. Andrews, A. Guha, M. Iacocca, B.P. O'Neill, G. Foltz, J. Myers, D.J. Weisenberger, R. Penny, R. Kucherlapati, C.M. Perou, D.N. Hayes, R. Gibbs, M. Marra, G.B. Mills, E. Lander, P. Spellman, R. Wilson, C. Sander, J. Weinstein, M. Meyerson, S. Gabriel, P.W. Laird, D. Haussler, G. Getz, L. Chin, C. Benz, J. Barnholtz-Sloan, W. Barrett, Q. Ostrom, Y. Wolinsky, K.L. Black, B. Bose, P.T. Boulos, M. Boulos, J. Brown, C. Czerinski, M. Eppley, M. Iacocca, T. Kempista, T. Kitko, Y. Koyfman, B. Rabeno, P. Rastogi, M. Sugarman, P. Swanson, K. Yalamanchii, I.P. Otey, Y.S. Liu, Y. Xiao, J.T. Auman, P.-C. Chen, A. Hadjipanayis, E. Lee, S. Lee, P.J. Park, J. Seidman, L. Yang, R. Kucherlapati, S. Kalkanis, T. Mikkelsen, L.M. Poisson, A. Raghunathan, L. Scarpace, B. Bernard, R. Bressler, A. Eakin, L. Iype, R.B. Kreisberg, K. Leinonen, S. Reynolds, H. Rovira, V. Thorsson, I. Shmulevich, M.J. Annala, R. Penny, J. Paulauskis, E. Curley, M. Hatfield, D. Mallery, S. Morris, T. Shelton, C. Shelton, M. Sherman, P. Yena, L. Cuppini, F. DiMeco, M. Eoli, G. Finocchiaro, E. Maderna, B. Pollo, M. Saini, S. Balu, K.A. Hoadley, L. Li, C.R. Miller, Y. Shi, M.D. Topal, J. Wu, G. Dunn, C. Giannini, B.P. O'Neill, B.A. Aksoy, Y. Antipin, L. Borsu, S.H. Berman, C.W. Brennan, E. Cerami, D. Chakravarty, G. Ciriello, J. Gao, B. Gross, A. Jacobsen, M. Ladanyi, A. Lash, Y. Liang, B. Reva, C. Sander, N. Schultz, R. Shen, N.D. Socci, A. Viale, M.L. Ferguson, Q.-R. Chen, J.A. Demchok, L.A.L. Dillon, K.R.M. Shaw, M. Sheth, R. Tarnuzzer, Z. Wang, L. Yang, T. Davidsen, M.S. Guyer, B.A. Ozenberger, H.J. Sofia, J. Bergsten, J. Eckman, J. Harr, J. Myers, C. Smith, K. Tucker, C. Winemiller, L.A. Zach, J.Y. Ljubimova, G. Eley, B. Ayala, M.A. Jensen, A. Kahn, T.D. Pihl, D.A. Pot, Y. Wan, J. Eschbacher, G. Foltz, N. Hansen, P. Hothi, B. Lin, N. Shah, J. Yoon, C. Lau, M. Berens, K. Ardlie, R. Beroukhim, S.L. Carter, A.D. Cherniack, M. Noble, J. Cho, K. Cibulskis, D. DiCara, S. Frazer, S.B. Gabriel, N. Gehlenborg, J. Gentry, D. Heiman, J. Kim, R. Jing, E.S. Lander, M. Lawrence, P. Lin, W. Mallard, M. Meyerson, R.C. Onofrio, G. Saksena, S. Schumacher, C. Sougnez, P. Stojanov, B. Tabak, D. Voet, H. Zhang, L. Zou, G. Getz, N.N. Dees, L. Ding, L.L. Fulton, R.S. Fulton, K.-L. Kanchi, E.R. Mardis, R.K. Wilson, S.B. Baylin, D.W. Andrews, L. Harshyne, M.L. Cohen, K. Devine, A.E. Sloan, S.R. VandenBerg, M.S. Berger, M. Prados, D. Carlin, B. Craft, K. Ellrott, M. Goldman, T. Goldstein, M. Grifford, D. Haussler, S. Ma, S. Ng, S.R. Salama, J.Z. Sanborn, J. Stuart, T. Swatloski, P. Waltman, J. Zhu, R. Foss, B. Frentzen, W. Friedman, R. McTiernan, A. Yachnis, D.N. Hayes, C.M. Perou, S. Zheng, R. Vegesna, Y. Mao, R. Akbani, K. Aldape, O. Bogler, G.N. Fuller, W. Liu, Y. Liu, Y. Lu, G. Mills, A. Protopopov, X. Ren, Y. Sun, C.-J. Wu, W.K.A. Yung, W. Zhang, J. Zhang, K. Chen, J.N. Weinstein, L. Chin, R.G.W. Verhaak, H. Noushmehr, D.J. Weisenberger, M.S. Bootwalla, P.H. Lai, T.J. Triche, D.J. Van Den Berg, P.W. Laird, D.H. Gutmann, N.L. Lehman, E.G. VanMeir, D. Brat, J.J. Olson, G.M. Mastrogianakis, N.S. Devi, Z. Zhang, D. Bigner, E. Lipp, R. McLendon, The somatic genomic landscape of glioblastoma, Cell 155 (2013) 462–477, https://doi.org/10.1016/j.cell.2013.09.034.
[31] N. Bergmann, C. Delbridge, J. Gempt, A. Feuchtinger, A. Walch, L. Schirmer, W. Bunk, T. Aschenbrenner, F. Liesche-Starnecker, J. Schlegel, The intratumoral heterogeneity reflects the intertumoral subtypes of glioblastoma multiforme: a regional immunohistochemistry analysis, Front. Oncol. 10 (2020), https://doi.org/10.3389/fonc.2020.00494.
[32] J. Cox, M. Mann, MaxQuant enables high peptide identification rates, individualized p.p.b.-range mass accuracies and proteome-wide protein quantification, Nat. Biotechnol. 26 (2008) 1367–1372, https://doi.org/10.1038/nbt.1511.
[33] K. Weke, A. Singh, N. Uwugiaren, J.A. Alfaro, T. Wang, T.R. Hupp, J.R. O'Neill, B. Vojtesek, D.R. Goodlett, S.M. Williams, M. Zhou, R.T. Kelly, Y. Zhu, I. Dapic, MicroPOTS analysis of barrett's esophageal cell line models identifies proteomic changes after physiologic and radiation stress, J. Proteome Res. 20 (2021) 2195–2205, https://doi.org/10.1021/acs.jproteome.0c00629.
[34] A.T. Kong, F.V. Leprevost, D.M. Avtonomov, D. Mellacheruvu, A.I. Nesvizhskii, MSFragger: ultrafast and comprehensive peptide identification in mass spectrometry–based proteomics, Nat. Methods 14 (2017) 513–520, https://doi.org/10.1038/nmeth.4256.
[35] V. Demichev, C.B. Messner, S.I. Vernardis, K.S. Lilley, M. Ralser, Dia-Nn, Neural networks and interference correction enable deep proteome coverage in high throughput, Nat. Methods 17 (2020) 41–44, https://doi.org/10.1038/s41592-019-0638-x.
[36] Y. Perez-Riverol, A. Csordas, J. Bai, M. Bernal-Llinares, S. Hewapathirana, D.J. Kundu, A. Inuganti, J. Griss, G. Mayer, M. Eisenacher, E. Pérez, J. Uszkoreit, J. Pfeuffer, T. Sachsenberg, Ş. Yılmaz, S. Tiwary, J. Cox, E. Audain, M. Walzer, A.F. Jarnuczak, T. Ternent, A. Brazma, J.A. Vizcaíno, The PRIDE database and related tools and resources in 2019: improving support for quantification data, Nucleic Acids Res 47 (2019) D442–D450, https://doi.org/10.1093/nar/gky1106.
[37] I. Dapic, N. Uwugiaren, P.J. Jansen, G.L. Corthals, Fast and simple protocols for mass spectrometry-based proteomics of small fresh frozen uterine tissue

sections, Anal. Chem. 89 (2017) 10769–10775, https://doi.org/10.1021/acs.analchem.7b01937.
[38] J. Tang, D. He, P. Yang, J. He, Y. Zhang, Genome-wide expression profiling of glioblastoma using a large combined cohort, Sci. Rep. 8 (2018) 15104, https://doi.org/10.1038/s41598-018-33323-z.
[39] M. Liu, Z. Xu, Z. Du, B. Wu, T. Jin, K. Xu, L. Xu, E. Li, H. Xu, The identification of key genes and pathways in glioma by bioinformatics analysis, J. Immunol. Res. 2017 (2017), e1278081, https://doi.org/10.1155/2017/1278081.
[40] W.-Q. Wang, O.N. Jensen, I.M. Møller, K.H. Hebelstrup, A. Rogowska-Wrzesinska, Evaluation of sample preparation methods for mass spectrometry-based proteomic analysis of barley leaves, Plant Methods 14 (2018) 72, https://doi.org/10.1186/s13007-018-0341-4.
[41] A. Hu, W.S. Noble, A. Wolf-Yadlin, Technical advances in proteomics: new developments in data-independent acquisition, F1000Research 5 (2016), F1000, https://doi.org/10.12688/f1000research.7042.1. Faculty Rev-419.
[42] Y.S. Ting, J.D. Egertson, J.G. Bollinger, B.C. Searle, S.H. Payne, W.S. Noble, M.J. MacCoss, PECAN: library-free peptide detection for data-independent acquisition tandem mass spectrometry data, Nat. Methods 14 (2017) 903–908, https://doi.org/10.1038/nmeth.4390.
[43] L.C. Gillet, P. Navarro, S. Tate, H. Röst, N. Selevsek, L. Reiter, R. Bonner, R. Aebersold, Targeted data extraction of the MS/MS spectra generated by data-independent acquisition: a new concept for consistent and accurate proteome analysis, Mol. Cell. Proteomics 11 (2012), https://doi.org/10.1074/mcp.O111.016717.
[44] P. Wei, W. Zhang, L.-S. Yang, H.-S. Zhang, X.-E. Xu, Y.-H. Jiang, F.-P. Huang, Q. Shi, Serum GFAP autoantibody as an ELISA-detectable glioma marker, Tumor Biol 34 (2013) 2283–2292, https://doi.org/10.1007/s13277-013-0770-7.
[45] Z. Zhuang, M. Qi, J. Li, H. Okamoto, D.S. Xu, R.R. Iyer, J. Lu, C. Yang, R.J. Weil, A. Vortmeyer, R.R. Lonser, Proteomic identification of glutamine synthetase as a differential marker for oligodendrogliomas and astrocytomas, J. Neurosurg. 115 (2011) 789–795, https://doi.org/10.3171/2011.5.JNS11451.
[46] M.J.H.M. Herpers, H. Budka, Glial fibrillary acidic protein (GFAP) in oligodendroglial tumors: gliofibrillary oligodendroglioma and transitional oligoastrocytoma as subtypes of oligodendroglioma, Acta Neuropathol. 64 (1984) 265–272, https://doi.org/10.1007/BF00690392.
[47] C. Thirant, P. Varlet, J. Lipecka, M.L. Gall, C. Broussard, P. Chafey, J.-M. Studler, J. Lacombe, S. Lions, A. Guillaudeau, L. Camoin, C. Daumas-Duport, M.-P. Junier, H. Chneiweiss, Proteomic analysis of oligodendrogliomas expressing a mutant isocitrate dehydrogenase-1, Proteomics 11 (2011) 4139–4154, https://doi.org/10.1002/pmic.201000646.
[48] A.K. Anagnostopoulos, K.S. Dimas, C. Papathanassiou, M. Braoudaki, E. Anastasiadou, K. Vougas, K. Karamolegou, H. Kontos, N. Prodromou, F. Tzortzatou-Stathopoulou, G.Th Tsangaris, Proteomics studies of childhood pilocytic astrocytoma, J. Proteome Res. 10 (2011) 2555–2565, https://doi.org/10.1021/pr200024m.
[49] L.-B. Wang, A. Karpova, M.A. Gritsenko, J.E. Kyle, S. Cao, Y. Li, D. Rykunov, A. Colaprico, J.H. Rothstein, R. Hong, V. Stathias, M. Cornwell, F. Petralia, Y. Wu, B. Reva, K. Krug, P. Pugliese, E. Kawaler, L.K. Olsen, W.-W. Liang, X. Song, Y. Dou, M.C. Wendl, W. Caravan, W. Liu, D.C. Zhou, J. Ji, C.-F. Tsai, V.A. Petyuk, J. Moon, W. Ma, R.K. Chu, K.K. Weitz, R.J. Moore, M.E. Monroe, R. Zhao, X. Yang, S. Yoo, A. Krek, A. Demopoulos, H. Zhu, M.A. Wyczalkowski, J.F. McMichael, B.L. Henderson, C.M. Lindgren, H. Boekweg, S. Lu, J. Baral, L. Yao, K.G. Stratton, L.M. Bramer, E. Zink, S.P. Couvillion, K.J. Bloodsworth, S. Satpathy, W. Sieh, S.M. Boca, S. Schürer, F. Chen, M. Wiznerowicz, K.A. Ketchum, E.S. Boja, C.R. Kinsinger, A.I. Robles, T. Hiltke, M. Thiagarajan, A.I. Nesvizhskii, B. Zhang, D.R. Mani, M. Ceccarelli, X.S. Chen, S.L. Cottingham, Q.K. Li, A.H. Kim, D. Fenyö, K.V. Ruggles, H. Rodriguez, M. Mesri, S.H. Payne, A.C. Resnick, P. Wang, R.D. Smith, A. Iavarone, M.G. Chheda, J.S. Barnholtz-Sloan, K.D. Rodland, T. Liu, L. Ding, A. Agarwal, M. Amin, E. An, M.L. Anderson, D.W. Andrews, T. Bauer, C. Birger, M.J. Birrer, L. Blumenberg, W.E. Bocik, U. Borate, M. Borucki, M.C. Burke, S. Cai, A.P. Calinawan, S.A. Carr, S. Cerda, D.W. Chan, A. Charamut, L.S. Chen, D. Chesla, A.M. Chinnaiyan, S. Chowdhury, M.P. Cieślik, D.J. Clark, H. Culpepper, T. Czernicki, F. D'Angelo, J. Day, S.D. Young, E. Demir, S.M. Dhanasekaran, R. Dhir, M.J. Domagalski, B. Druker, E. Duffy, M. Dyer, N.J. Edwards, R. Edwards, K. Elburn, M.J. Ellis, J. Eschbacher, A. Francis, S. Gabriel, N. Gabrovski, L. Garofano, G. Getz, M.A. Gillette, A.K. Godwin, D. Golbin, Z. Hanhan, L.I. Hannick, P. Hariharan, B. Hindenach, K.A. Hoadley, G. Hostetter, C. Huang, E. Jaehnig, S.D. Jewell, N. Ji, C.D. Jones, A. Karz, W. Kaspera, L. Kim, R.B. Kothadia, C. Kumar-Sinha, J. Lei, F.D. Leprevost, K. Li, Y. Liao, J. Lilly, H. Liu, J. Lubínski, R. Madan, W. Maggio, E. Malc, A. Malovannaya, S. Mareedu, S.P. Markey, A. Marrero-Oliveras, N. Martinez, N. Maunganidze, J.E. McDermott, P.B. McGarvey, J. McGee, P. Mieczkowski, S. Migliozzi, F. Modugno, R. Montgomery, C.J. Newton, G.S. Omenn, U. Ozbek, O.V. Paklina, A.G. Paulovich, A.M. Perou, A.R. Pico, P.D. Piehowski, D.G. Placantonakis, L. Polonskaya, O. Potapova, B. Pruetz, L. Qi, S. Ramkissoon, A. Resnick, S. Richey, G. Riggins, K. Robinson, N. Roche, D.C. Rohrer, B.R. Rood, L. Rossell, S.R. Savage, E.E. Schadt, Y. Shi, Z. Shi, Y. Shutack, S. Singh, T. Skelly, L.J. Sokoll, J. Stawicki, S.E. Stein, J. Suh, W. Szopa, D. Tabor, D. Tan, D. Tansil, R.R. Thangudu, C. Tognon, E. Traer, S. Tsang, J. Tyner, K.S. Um, D.R. Valley, S. Vasaikar, N. Vatanian, U. Velvulou, M. Vernon, W. Wan, J. Wang, A. Webster, B. Wen, J.R. Whiteaker, G.D. Wilson, Y. Zakhartsev, R. Zelt, H. Zhang, L. Zhang, Z. Zhang, G. Zhao, J. Zhu, Proteogenomic and metabolomic characterization of human glioblastoma, Cancer Cell 39 (2021) 509–528, https://doi.org/10.1016/j.ccell.2021.01.006, e20.
[50] J.-M. Lemée, A. Clavreul, M. Aubry, E. Com, M. de Tayrac, J. Mosser, P. Menei, Integration of transcriptome and proteome profiles in glioblastoma: looking for the missing link, BMC Mol. Biol. 19 (2018) 13, https://doi.org/10.1186/s12867-018-0115-6.
[51] J. Bathke, A. Konzer, B. Remes, M. McIntosh, G. Klug, Comparative analyses of the variation of the transcriptome and proteome of Rhodobacter sphaeroides throughout growth, BMC Genom. 20 (2019) 358, https://doi.org/10.1186/s12864-019-5749-3.
[52] L. Giusti, C. Angeloni, A. Lucacchini, Update on proteomic studies of formalin-fixed paraffin-embedded tissues, Expert Rev. Proteomics 16 (2019) 513–520, https://doi.org/10.1080/14789450.2019.1615452.
[53] I. Dapic, L. Baljeu-Neuman, N. Uwugiaren, J. Kers, D.R. Goodlett, G.L. Corthals, Proteome analysis of tissues by mass spectrometry, Mass Spectrom. Rev. 38 (2019) 403–441, https://doi.org/10.1002/mas.21598.
[54] O.J.R. Gustafsson, G. Arentz, P. Hoffmann, Proteomic developments in the analysis of formalin-fixed tissue, Biochim. Biophys. Acta BBA - Proteins Proteomics 1854 (2015) 559–580, https://doi.org/10.1016/j.bbapap.2014.10.003.
[55] Y. Kawashima, E. Watanabe, T. Umeyama, D. Nakajima, M. Hattori, K. Honda, O. Ohara, Optimization of data-independent acquisition mass spectrometry for deep and highly sensitive proteomic analysis, Int. J. Mol. Sci. 20 (2019) 5932, https://doi.org/10.3390/ijms20235932.
[56] S. Oh, J. Yeom, H.J. Cho, J.-H. Kim, S.-J. Yoon, H. Kim, J.K. Sa, S. Ju, H. Lee, M.J. Oh, W. Lee, Y. Kwon, H. Li, S. Choi, J.H. Han, J.H. Chang, E. Choi, J. Kim, N.-G. Her, S.H. Kim, S.-G. Kang, E. Paek, D.-H. Nam, C. Lee, H.S. Kim, Integrated pharmacoproteogenomics defines two subgroups in isocitrate dehydrogenase wild-type glioblastoma with prognostic and therapeutic opportunities, Nat. Commun. 11 (2020) 3288, https://doi.org/10.1038/s41467-020-17139-y.
[57] G. La Rocca, G.A. Simboli, F. Vincenzoni, D.V. Rossetti, A. Urbani, T. Ius, G.M. Della Pepa, A. Olivi, G. Sabatino, C. Desiderio, Glioblastoma CUSA fluid protein profiling: a comparative investigation of the core and peripheral tumor zones, Cancers 13 (2021) 30, https://doi.org/10.3390/cancers13010030.
[58] Y.-C. Song, G.-X. Lu, H.-W. Zhang, X.-M. Zhong, X.-L. Cong, S.-B. Xue, R. Kong, D. Li, Z.-Y. Chang, X.-F. Wang, Y.-J. Zhang, R. Sun, L. Chai, R.-T. Xie, M.-X. Cai, M. Sun, W.-Q. Mao, H.-Q. Yang, Y.-C. Shao, S.-Y. Fan, T.-M. Wu, Q. Xia, Z.-W. Lv, D.A. Fu, Y.-S. Ma, Proteogenomic characterization and integrative analysis of glioblastoma multiforme, Oncotarget 8 (2017) 97304–97312, https://doi.org/10.18632/oncotarget.21937.
[59] S. Ye, J. Wu, Y. Wang, Y. Hu, T. Yin, J. He, Quantitative proteomics analysis of glioblastoma cell lines after lncRNA HULC silencing, Sci. Rep. 11 (2021), 12587, https://doi.org/10.1038/s41598-021-92089-z.
[60] K.H.B. Lam, A.J. Leon, W. Hui, S.C.-E. Lee, I. Batruch, K. Faust, A. Klekner, G. Hutóczki, M. Koritzinsky, M. Richer, U. Djuric, P. Diamandis, Topographic mapping of the glioblastoma proteome reveals a triple-axis model of intratumoral heterogeneity, Nat. Commun. 13 (2022) 116, https://doi.org/10.1038/s41467-021-27667-w.
[61] M.J.H.M. Herpers, F.C.S. Ramaekers, J. Aldeweireldt, O. Moesker, J. Slooff, Co-expression of glial fibrillary acidic protein- and vimentin-type intermediate filaments in human astrocytomas, Acta Neuropathol. 70 (1986) 333–339, https://doi.org/10.1007/BF00686093.
[62] J. Zhao, L. Zhang, X. Dong, L. Liu, L. Huo, H. Chen, High expression of vimentin is associated with progression and a poor outcome in glioblastoma, Appl. Immunohistochem. Mol. Morphol. 26 (2018) 337–344, https://doi.org/10.1097/PAI.0000000000000420.
[63] H. Tang, Y. Wang, B. Zhang, S. Xiong, L. Liu, W. Chen, G. Tan, H. Li, High brain acid soluble protein 1(BASP1) is a poor prognostic factor for cervical cancer and promotes tumor growth, Cancer Cell Int 17 (2017) 97, https://doi.org/10.1186/s12935-017-0452-4.
[64] Q. Zhou, R. Andersson, D. Hu, M. Bauden, T. Kristl, A. Sasor, K. Pawłowski, I. Pla, K.S. Hilmersson, M. Zhou, F. Lu, G. Marko-Varga, D. Ansari, Quantitative proteomics identifies brain acid soluble protein 1 (BASP1) as a prognostic biomarker candidate in pancreatic cancer tissue, EBioMedicine 43 (2019) 282–294, https://doi.org/10.1016/j.ebiom.2019.04.008.
[65] S.K. Akiyama, K. Olden, K.M. Yamada, Fibronectin and integrins in invasion and metastasis, Cancer Metastasis Rev 14 (1995) 173–189, https://doi.org/10.1007/BF00690290.
[66] T. Ohnishi, S. Hiraga, S. Izumoto, H. Matsumura, Y. Kanemura, N. Arita, T. Hayakawa, Role of fibronectin-stimulated tumor cell migration in glioma invasion in vivo: clinical significance of fibronectin and fibronectin receptor expressed in human glioma tissues, Clin. Exp. Metastasis 16 (1998) 729–741, https://doi.org/10.1023/A:1006532812408.
[67] T.J. Alban, D. Bayik, B. Otvos, A. Rabljenovic, L. Leng, L. Jia-Shiun, G. Roversi, A. Lauko, A.A. Momin, A.M. Mohammadi, D.M. Peereboom, M.S. Ahluwalia, K. Matsuda, K. Yun, R. Bucala, M.A. Vogelbaum, J.D. Lathia, Glioblastoma myeloid-derived suppressor cell subsets express differential macrophage migration inhibitory factor receptor profiles that can Be targeted to reduce immune suppression, Front. Immunol. 11 (2020) 1191, https://doi.org/10.3389/fimmu.2020.01191.
[68] W. Ha, H. Sevim-Nalkiran, A.M. Zaman, K. Matsuda, M. Khasraw, A.K. Nowak, L. Chung, R.C. Baxter, K.L. McDonald, Ibudilast sensitizes glioblastoma to temozolomide by targeting macrophage migration inhibitory factor (MIF), Sci. Rep. 9 (2019) 2905, https://doi.org/10.1038/s41598-019-39427-4.